Chapter 1

UNDERSTANDING RADIATIVE-CAPTURE REACTIONS AT VERY LOW ENERGIES

Daniel Baye*
Physique Quantique C.P. 165/82, and
Physique Nucléaire Théorique et Physique Mathématique, C.P. 229,
Université Libre de Bruxelles (ULB), B 1050 Brussels, Belgium

Abstract

Radiative-capture reactions are studied in the potential model at very low energies including energy zero. For the capture of charged particles, the astrophysical S factor possesses a Taylor expansion in powers of the energy of the relative motion. By using scaled scattering functions with a finite non-zero limit at energy zero, the S factor is obtained in the potential model from a simple integral which allows visualizing its behaviour at energies close to zero. The first coefficients of this expansion can be calculated accurately from solutions of the Schrödinger equation and its derivatives with respect to energy, at energy zero. The ^{3}He(α,γ)^{7}Be and ^{7}Be(p,γ)^{8}B reactions are used as illustrative examples. The same approach applies to the proton-proton weak capture. For neutron radiative capture, the product σv of the capture cross section and the relative velocity also possesses a Taylor expansion in powers of the energy, which can be treated in a similar way. The neutron capture by ^{12}C, ^{14}C and ^{16}O are used as examples. The extension of these treatments to microscopic models of radiative capture is discussed in the context of the R-matrix theory.

PACS 25.40.Lw, 24.50.+g, 28.20.Fc, 26.20.Cd.

Keywords: Radiative capture, low energies, potential model, S factor.

*E-mail address: dbaye@ulb.ac.be

1. Introduction

The determination of accurate radiative-capture cross sections is a fundamental problem in astrophysics [1, 2, 3]. These reactions play an essential role in the synthesis of elements and in particular of the light elements appearing in the sun through the pp chains. The rates of these reactions are crucial for understanding the evolution of stars. In most burning conditions in stars, the temperatures are very low in nuclear scales. The reactions between charged particles occur in general far below the Coulomb barrier.

Radiative capture is nothing but an electromagnetic transition between a continuum state and a bound state. It is more complicated than usual transitions in bound spectra because the continuum state is not square integrable and depends on a parameter, the energy. The continuum state may involve resonances at some energies. Resonances play a dominant role in radiative captures of protons leading to heavier elements in the CNO cycle and beyond. In general, resonant capture allows a simple approximate treatment. Here I focus on non-resonant capture mostly encountered with light elements and its understanding. This process is often called direct capture but this name can be misleading since resonant capture can also be a direct process. It is sometimes incorrectly considered as always arising from the compound-nucleus mechanism, i.e. a much slower mechanism not valid for light nuclei.

Quantum mechanics is essential to explain the radiative-capture cross sections at low energies thanks to tunneling through the Coulomb barrier. Hence the radiative-capture process is one of the simplest examples where one can observe wave functions at work. The basic ingredient of the calculation of cross sections contains the overlap between a scattering wave function describing the collision of two nuclei and the bound-state wave function of the nucleus created by their fusion. At a low energy of the relative motion, the scattering wave functions must be obtained in a situation where the Coulomb force dominates the stronger nuclear force. This unusual situation leads to very small cross sections, for which direct measurements are in general impossible in the energy range important for astrophysics. Hence a theoretical input is indispensable but, in most cases, impossible to verify experimentally. It is thus crucial to have a good physical understanding of the mechanism of the radiative-capture reactions.

An important present goal for nuclear physics is to obtain the cross sections of astrophysical interest from *ab initio* calculations, i.e. based on a model-independent solution of a many-body Schrödinger equation involving realistic nucleon-nucleon and multinucleon forces. Such calculations are in progress but do not provide an intuitive picture of the behaviour of cross sections, or more practically of the corresponding astrophysical S factor, a quantity derived from the cross section presenting a much weaker variation with respect to energy after the elimination of the main part of the barrier penetration effect. The simple potential model, also called direct-capture model, can provide such an intuitive picture in many cases by allowing us to visualize the energy dependence of the crucial matrix elements. Of course, it presents several simplifications such as the neglect of antisymmetrization [4] and a model dependence through the use of a more or less empirical nucleon-nucleus or nucleus-nucleus interaction. An even stronger model assumption is that the final bound state of the fused nucleus must be described as a two-body bound state of the initial colliding nuclei. In spite of these drawbacks, the potential model can provide a qualitative understanding of several radiative-capture processes through simple pictures. It

also allows a simple calculation of the behaviour of the S factor around zero energy that paves the way to similar calculations in more elaborate models.

The aim of the present chapter is to describe the properties of the potential model at very low energies in a pedagogical way. The results presented at very low energies and, in particular, at energy zero can be reproduced with little numerical effort and provide simple exercises for beginners in this field. They should represent a good training before studies with more elaborate models. This approach is also hoped to lead to more transparent physical interpretations of results obtained from microscopic models.

The rules of the game are presented in section 2. with the definitions of the astrophysical S factor and of the Gamow peak. In section 3., the expressions of the radiative-capture cross sections are given and the potential model is introduced. The radiative capture of charged particles is discussed in section 4.. A brief parenthesis in section 5. shows that the proton-proton weak capture can be explained with the same scheme. Neutron radiative capture is addressed in section 6.. The R-matrix approach which provides a link with more elaborate models is briefly described in section 7.. A conclusion is presented in section 8..

2. Astrophysical S factor and Gamow peak

A reaction involving two nuclei with charges Z_1e and Z_2e and masses A_1 and A_2 takes place at the relative velocity v. The energy of their relative motion is

$$E = \frac{1}{2}\mu v^2 = \frac{\hbar^2 k^2}{2\mu}, \tag{1}$$

where μ is the reduced mass of the nuclei and k is the wave number. Let us start with the case of a capture of charged particles ($Z_1Z_2 \neq 0$). The neutron capture requires a separate treatment (see section 6.).

When both particles are charged, the Coulomb repulsion hinders reactions at energies below the top E_B of the Coulomb barrier. The order of magnitude of the penetration probability into the Coulomb barrier is roughly given by the Gamow factor

$$\exp(-2\pi\eta), \tag{2}$$

where η is the Sommerfeld parameter

$$\eta = \frac{Z_1Z_2e^2}{\hbar v} = \sqrt{\frac{E_N}{E}}. \tag{3}$$

The second expression of η involves the nuclear Rydberg energy

$$E_N = \frac{1}{2}(Z_1Z_2\alpha)^2\mu c^2 = \frac{\hbar^2}{2\mu a_N^2} \tag{4}$$

where $\alpha = e^2/\hbar c$ is the fine structure constant and a_N is the nuclear Bohr radius

$$a_N = \frac{\hbar^2}{\mu Z_1 Z_2 e^2}. \tag{5}$$

The nuclear Bohr radius and Rydberg energy are natural units for collision between charged nuclei below the Coulomb barrier. The Sommerfeld parameter is inversely proportional to the square root of the energy and increases thus when $E \to 0$. The product ηk is independent of the energy,

$$\eta k = \frac{1}{a_N}. \tag{6}$$

The Gamow factor is a fast decreasing function when E decreases. It does not possess a Taylor expansion around $E = 0$.

Reaction cross sections $\sigma(E)$ and, in particular, radiative-capture cross sections decrease very fast when the energy tends to zero, following roughly the behaviour of the Gamow factor. They do not possess a Taylor expansion around $E = 0$. It is convenient to introduce another quantity, the astrophysical S factor, which varies much less rapidly at low energy than the cross section (outside resonances, if any). It is defined by

$$S(E) = Ee^{2\pi\eta}\sigma(E). \tag{7}$$

As explained below, it has the interesting property of having a finite non-zero limit for $E \to 0$ and a Taylor expansion around this energy,

$$S(E) = S(0) + S'(0)E + \tfrac{1}{2}S''(0)E^2 + \ldots \tag{8}$$

with $S(0) \neq 0$. This property allows studying the behaviour of the S factor at energies arbitrarily close to zero.

In models of the chemical evolution of some astrophysical system, the crucial information is given by the reaction rate per particle pair [1]

$$\langle \sigma v \rangle = \left(\frac{1}{\pi\mu}\right)^{1/2} \left(\frac{2}{k_{\rm B}T}\right)^{3/2} \int_0^\infty e^{-E/k_{\rm B}T} e^{-2\pi\eta} S(E) dE, \tag{9}$$

where $k_{\rm B}$ is the Boltzmann constant and T is the temperature. The integrand contains two fast varying factors in addition to the slowly varying astrophysical S factor. It is convenient to study separately the behaviour of the fast varying factors. The function

$$g(E) = e^{-E/k_{\rm B}T} e^{-2\pi\sqrt{E_N/E}} \tag{10}$$

is depicted in Fig. 1. Its shape is known as the Gamow peak. It displays a maximum at the energy

$$E_0 = \left(\pi k_{\rm B} T \sqrt{E_N}\right)^{2/3}. \tag{11}$$

This energy is known as the most efficient energy [1] although the true maximum of the integrand in Eq. (9) may be slightly different due to the energy dependence of $S(E)$. It is customary to express this energy in MeV as a function of the temperature in billion degrees $T_9 = T/10^9$ K as

$$E_0 \approx 0.122\ (Z_1^2 Z_2^2 A_1 A_2/A)^{1/3} T_9^{2/3}\ \text{MeV}. \tag{12}$$

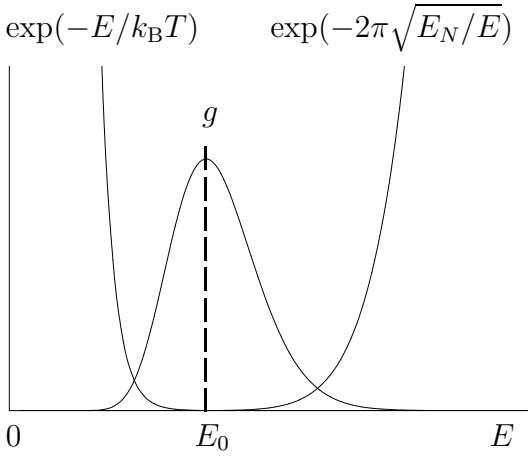

Figure 1. Gamow peak.

This expression is however not intuitive. A better understanding is obtained by comparing it with the energy E_B of the Coulomb barrier. This energy is conveniently approximated as

$$E_B \approx 0.9 \, \frac{Z_1 Z_2}{A_1^{1/3} + A_2^{1/3}} \, \mathrm{MeV}. \tag{13}$$

For proton and α capture by light nuclei, the ratio of E_0 to E_B is roughly given by

$$\frac{E_0}{E_B} \approx 0.3 \, T_9^{2/3}. \tag{14}$$

This approximate ratio has the merit to clearly show that capture takes place far below the Coulomb barrier for $T_9 < 1$.

If physics was classical, capture would be impossible below the Coulomb barrier. It could still occur through the high-energy tail of the Boltzmann distribution. The integral in (9) would start from E_B in place of 0 and the corresponding reaction rate would be proportional to an exponential involving the Coulomb barrier energy E_B,

$$\langle \sigma v \rangle_{\rm cl.} \propto e^{-E_B/k_{\rm B}T}. \tag{15}$$

But the real world obeys the laws of quantum physics and the tunneling through the Coulomb barrier leads with Eq. (9) to

$$\langle \sigma v \rangle \propto g(E_0) = e^{-3E_0/k_{\rm B}T}. \tag{16}$$

As shown by the ratio (14), the quantum reaction rate is much larger for $T_9 < 1$. If a resonance occurs at energies below the Coulomb barrier, it is narrow and leads to a contribution to the rate proportional to an exponential involving the resonance energy E_r,

$$\langle \sigma v \rangle_{\rm res.} \propto e^{-E_r/k_{\rm B}T}. \tag{17}$$

The rate can thus be significantly enhanced by resonances below or around the Gamow peak.

The crucial ingredient for understanding the value of the reaction rate is the coefficient of $g(E_0)$ in Eq. (16) which depends on the value of $S(E_0)$. More precisely, the reaction rate depends on the values of $S(E)$ in the Gamow-peak domain. The study of the properties of the astrophysical S factor for non resonant radiative-capture reactions at very low energies is the main topic of this chapter.

3. Radiative-capture models

3.1. General model cross sections

Let us consider a capture process where two nuclei with respective masses A_1 and A_2 and charges Z_1e and Z_2e fuse into a nucleus with mass A and charge Ze by emitting a photon with wave number k_γ. Let I_1 and I_2 be the total internal angular momenta of the colliding nuclei and I be a result of their coupling, known as the channel spin. The final bound state is characterized by two good quantum numbers, its total angular momentum J_f and its parity π_f. The initial scattering state possesses an infinity of partial waves. The electromagnetic transition operator can be expanded into electric and magnetic multipoles. For each multipole, selection rules limit the number of active initial partial waves. Let l_i be the initial orbital angular momentum of the relative motion between the colliding nuclei in the entrance channel for a given partial wave and J_i be an initial total angular momentum resulting from the coupling of this relative orbital momentum with the channel spin I.

The bound-state wave function $\Psi^{J_f M_f \pi_f}$ of the final nucleus has energy $E^{J_f\pi_f}$ with respect to the elastic threshold. The transition operator $\mathcal{M}^{\sigma\lambda}_\mu$ with multipolarity λ corresponds to an electric transition for σ = E or a magnetic transition for σ = M. The radiative-capture cross section is given for example in Refs. [5, 6] as

$$\sigma_{J_f\pi_f}(E) = \frac{64\pi^4}{\hbar v}\frac{2J_f+1}{(2I_1+1)(2I_2+1)}\sum_{\sigma\lambda}\frac{k_\gamma^{2\lambda+1}}{[(2\lambda+1)!!]^2}\frac{\lambda+1}{\lambda} \times \sum_{l_i I J_i}\frac{1}{2l_i+1}|\langle\Psi^{J_f\pi_f}||\mathcal{M}^{\sigma\lambda}||\Psi^{J_i}_{l_i I}(E)\rangle|^2, \quad (18)$$

where $\Psi^{J_i M_i}_{l_i I}(E)$ is a partial wave of the initial scattering wave function at the energy E of the relative motion, with a specific normalization. The energy E_γ and wave number k_γ of the photon are given by

$$E_\gamma = \hbar c k_\gamma = E + Q - E_x \quad (19)$$

as a function of the Q value of the reaction and of the excitation energy E_x of the final nucleus. A small recoil term is neglected.

The capture cross section (18) involves a sum over all multipoles, electric and magnetic. For radiative capture, the emitted photons have energies smaller than 10 MeV in most cases and the long-wavelength approximation is valid. The sum over multipoles is dominated by the dipole term, except when it is forbidden by an isospin selection rule. When E1 is

forbidden, the dominant component is E2 although the forbidden E1 component may be of the same order of magnitude like in the ^{12}C$(\alpha,\gamma)^{16}$O reaction. The present study is thus restricted to electric multipole operators, with $\lambda = 1$ or 2 in practice.

Let $\boldsymbol{r}_p$ be the coordinates of proton p ($p = 1$ to Z) and $\boldsymbol{R}_{\rm cm}$ be the coordinate of the centre of mass of the system of A nucleons. The electric transition operators read at the long-wavelength approximation

$$\mathcal{M}^{{\rm E}\lambda}_{\mu} = e\sum_{p=1}^{Z} r'^{\lambda}_{p} Y_{\lambda\mu}(\Omega'_p) \tag{20}$$

where the sum runs over all protons. The operators depend on the relative coordinates $\boldsymbol{r}'_p = \boldsymbol{r}_p - \boldsymbol{R}_{\rm cm} = (r'_p, \Omega'_p)$ with respect to the centre of mass of the system of A nucleons.

Expression (18) is quite general. It is valid for microscopic models where all nucleons are taken into account and the wave functions are properly antisymmetrized. This covers the microscopic cluster model [5, 7] as well as recent or future *ab initio* calculations [8, 9]. In this chapter, the goal is understanding the radiative-capture process and its important properties are better seen on a much simpler model, the potential model [4, 10, 11, 12].

3.2. Potential model

In the potential model, the internal structure of the reacting nuclei is essentially neglected. They are treated as pointlike particles with a spin. The only quantal variable is then the relative coordinate $\boldsymbol{r} = (r, \Omega)$ between these nuclei. Their internal structure however determines the nucleus-nucleus interaction that is the main ingredient of the model. This local interaction can be phenomenological or derived from a more elaborate model. Antisymmetrization effects can even be partly simulated by introducing unphysical bound states in the potential. These deeply bound states allow obtaining wave functions with a node structure closer to the node structure of relative wave functions of more physical bound and scattering states derived in microscopic models.

The model is based on a local nucleus-nucleus potential involving nuclear and Coulomb components. The nuclear potential may contain a spin-orbit term involving for example a coupling of the orbital momentum with the channel spin I. A bound state is characterized by quantum numbers $l_f J_f$ and a scattering partial wave by quantum numbers $l_i J_i$ where the total angular momenta result from the coupling of the orbital momenta with I. In the potential model, I is both the channel spin of the scattering wave function and the total intrinsic spin of the final nucleus. The energy of the final nucleus with respect to the elastic threshold is denoted as $E_{l_f J_f}$.

After separation of the spin and angular components, the bound and scattering wave functions are described for a given orbital momentum l and total angular momentum J as eigenfunctions of the radial Schrödinger equation

$$H_{lJ} u_{lJ}(r) = E u_{lJ}(r), \tag{21}$$

with respective energies $E_{l_f J_f}$ and E. In Eq. (21), the radial Hamiltonian reads

$$H_{lJ} = -\frac{\hbar^2}{2\mu}\left[\frac{d^2}{dr^2} - \frac{l(l+1)}{r^2}\right] + V^{lJ}_{\rm N}(r) + V_{\rm C}(r), \tag{22}$$

where $V_{\rm N}^{lJ}(r)$ is the nuclear interaction between the clusters for the considered partial wave lJ and $V_{\rm C}(r)$ is the Coulomb interaction between them. Potential $V_{\rm C}$ usually differs from the Coulomb interaction $Z_1 Z_2 e^2/r$ between two point charges to partly take account of the finite size of the nuclei. It is, for example, a point-sphere Coulomb interaction. For neutron capture, the Coulomb potential $V_{\rm C}(r)$ vanishes.

For nuclei that can be considered as pointlike to a good approximation, the proton coordinates of nucleus 1 differ only slightly from the coordinate of the centre of mass of this nucleus with respect to the centre of mass of the full system,

$$\boldsymbol{r}'_p \approx -\frac{A_2}{A}\boldsymbol{r} \qquad\qquad (p = 1, \ldots, Z_1). \tag{23}$$

In the same way, the proton coordinates of nucleus 2 differ only slightly from the coordinate of the centre of mass of this nucleus with respect to the centre of mass of the system,

$$\boldsymbol{r}'_p \approx \frac{A_1}{A}\boldsymbol{r} \qquad\qquad (p = Z_1 + 1, \ldots, Z). \tag{24}$$

Hence the electric transition operators (20) take the approximate form

$$\mathcal{M}^{{\rm E}\lambda}_\mu \approx e Z^{{\rm E}\lambda}_{\rm eff} r^\lambda Y_{\lambda\mu}(\Omega), \tag{25}$$

where $Z^{{\rm E}\lambda}_{\rm eff}$ is an effective charge given by

$$Z^{{\rm E}\lambda}_{\rm eff} = Z_1 \left(-\frac{A_2}{A}\right)^\lambda + Z_2 \left(\frac{A_1}{A}\right)^\lambda. \tag{26}$$

It is always strictly positive for E2 but can vanish or be negative for E1.

The radiative-capture cross section in the potential model is a particular case of Eq. (18) where the wave functions depend on a single coordinate $\boldsymbol{r}$. It is given for example in Ref. [3]. Using the potential model wave functions of the initial and final states and approximation (25) for the transition operator, the cross section reads

$$\sigma^{{\rm E}\lambda}_{l_f J_f}(E) = \frac{\alpha c}{k^2 v}\, k_\gamma^{2\lambda+1} \sum_{l_i J_i} N^{{\rm E}\lambda}_{l_i J_i} \left[\int_0^\infty u_{l_f J_f}(r)\, r^\lambda\, u_{l_i J_i}(E, r)\, dr\right]^2. \tag{27}$$

It implies that the scattering wave functions are normalized according to

$$u_{lJ}(E, r) \underset{r\to\infty}{\to} \cos\delta_{lJ}(E) F_l(\eta, kr) + \sin\delta_{lJ}(E) G_l(\eta, kr) \tag{28}$$

where $F_l(\eta, kr)$ and $G_l(\eta, kr)$ are the regular and irregular Coulomb wave functions [13] and $\delta_{lJ}(E)$ is the nuclear (or additional) phase shift at energy E for partial wave lJ. In Eq. (27), the normalization factor is given by

$$N^{{\rm E}\lambda}_{l_i J_i} = 8\pi \left(Z^{{\rm E}\lambda}_{\rm eff}\right)^2 \frac{(\lambda+1)(2\lambda+1)}{\lambda(2\lambda+1)!!^2} \frac{(2J_i+1)(2J_f+1)(2l_i+1)(2l_f+1)}{(2I_1+1)(2I_2+1)} \times \begin{pmatrix} l_f & \lambda & l_i \\ 0 & 0 & 0 \end{pmatrix}^2 \begin{Bmatrix} J_f & l_f & I \\ l_i & J_i & \lambda \end{Bmatrix}^2. \tag{29}$$

The photon wave number is related to the initial energy E through

$$k_\gamma = (|E_{l_f J_f}| + E)/\hbar c. \tag{30}$$

These expressions are also valid for the neutral case with $\eta = 0$. The Coulomb functions then reduce to spherical Bessel functions [13] multiplied by kr.

4. Radiative capture of charged particles

4.1. Scattering functions for $E \to 0$

When E tends towards zero, η tends to infinity and the scattering wave functions normalized according to (28) tend to zero. This is illustrated in Fig. 2 where one can observe the fast decrease of the wave functions with decreasing energy at fixed r. This behaviour is the

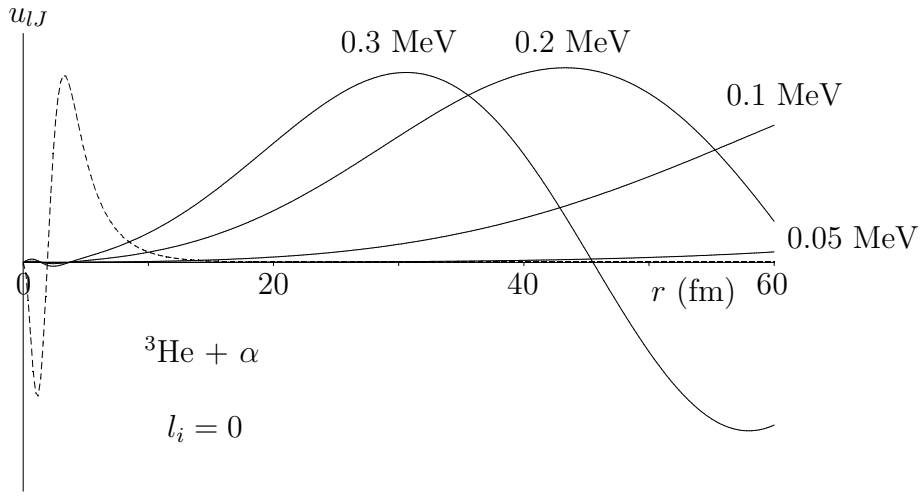

Figure 2. Radial wave functions $u_{0,1/2}(E,r)$ of the ^{3}He + α elastic collision normalized according to Eq. (28) at various low energies E. The final ground-state wave function $u_{1,3/2}(r)$ of ^{7}Be ($\times 2$) is represented as a dashed line.

consequence of the increase of the width of the Coulomb barrier when the energy tends to zero. Mathematically, it is a consequence of the normalization (28). Indeed, the regular function F_l tends to zero while the irregular function G_l tends to infinity.

$$F_l(\eta, kr) \sim e^{-\pi\eta} \underset{E\to 0}{\to} 0, \tag{31}$$

$$G_l(\eta, kr) \sim e^{+\pi\eta} \underset{E\to 0}{\to} \infty. \tag{32}$$

and the phase shifts tend to zero in such a way that

$$\delta_{lJ}(E) \underset{E\to 0}{\to} -2\pi \frac{a_{lJ}}{l!^2 a_N^{2l+1}}\, e^{-2\pi\eta} \underset{E\to 0}{\to} 0, \tag{33}$$

where a_{lJ} is the scattering length (see Appendix). Hence the asymptotic form (28) of $u_{lJ}(E,r)$ tends to zero when $E \to 0$,

$$u_{lJ}(E,r) \sim e^{-\pi\eta} \underset{E\to 0}{\to} 0, \tag{34}$$

for any r value.

The usual normalization of the Coulomb wave functions is not practical near $E = 0$. In order to avoid properties (31) and (32), scaled Coulomb functions are defined as [12]

$$\mathcal{F}_l(E,r) = k^{-1/2} e^{\pi\eta} F_l(\eta, kr) \tag{35}$$

and

$$\mathcal{G}_l(E,r) = \frac{\pi}{2} k^{-1/2} e^{-\pi\eta} G_l(\eta, kr). \tag{36}$$

Their advantage is that they have a finite limit when $E \to 0$. From the properties of the standard Coulomb functions [13], one deduces the Wronskian

$$W\{\mathcal{G}_l, \mathcal{F}_l\} = \pi/2, \tag{37}$$

where $W\{g,f\} = g(df/dr) - f(dg/dr)$. Through Eqs. (35) and (36), the scaled Coulomb functions are considered as directly depending on the energy E. In the following, primes are used to designate derivatives *with respect to energy*. For example, the first energy derivative of $\mathcal{F}_l$ is written as

$$\mathcal{F}'_l(E,r) = \frac{\partial}{\partial E} \mathcal{F}_l(E,r), \tag{38}$$

and similar expressions for other functions and derivatives.

A scaled scattering wave function $\widetilde{u}_{lJ}(E,r)$ can be defined as

$$\widetilde{u}_{lJ}(E,r) = k^{-1/2} e^{\pi\eta} u_{lJ}(E,r). \tag{39}$$

The asymptotic form of $\widetilde{u}_{lJ}(E,r)$ is given with the notations (35) and (36) by

$$\widetilde{u}_{lJ}(E,r) \underset{r\to\infty}{\to} \mathcal{F}_l(E,r) + \frac{2}{\pi} e^{2\pi\eta} \tan\delta_{lJ}(E) \mathcal{G}_l(E,r). \tag{40}$$

This normalization ensures that $\widetilde{u}_{lJ}$ has a finite limit when E tends towards zero [14, 12]. This behaviour is illustrated in Fig. 3. The wave functions now tend to a finite non-zero limit represented as a dotted line in the figure. This limit can be calculated by solving Eq. (63) below. While the $E = 0$ curve tends to infinity for $r \to \infty$, the curve at $E = 0.01$ MeV that looks very close starts to oscillate beyond the classical turning point at $Z_1 Z_2 e^2/E \approx 576$ fm, i.e. far beyond the range displayed in the figure. At large distances, the amplitude of the oscillations of the scattering wave functions $\widetilde{u}_{lJ}(E,r)$ with respect to r increases exponentially with $\exp(\pi\eta)$.

4.2. Potential-model expression of the astrophysical S factor

Rather than the radiative-capture cross section (27) in the potential model, it is easier to immediately use an expression for the S factor by absorbing the factors $E\exp(2\pi\eta)$ of Eq. (7) and $k^{-2}v^{-1}$ of Eq. (27) into the initial wave function [14]. The S factor for an electric transition of multipolarity λ to the final state $l_f J_f$ then reads

$$S^{\mathrm{E}\lambda}_{l_f J_f}(E) = \tfrac{1}{2}\alpha\hbar c k_\gamma^{2\lambda+1} \sum_{l_i J_i} N^{\mathrm{E}\lambda}_{l_i J_i} [I_{l_i J_i}(E)]^2. \tag{41}$$

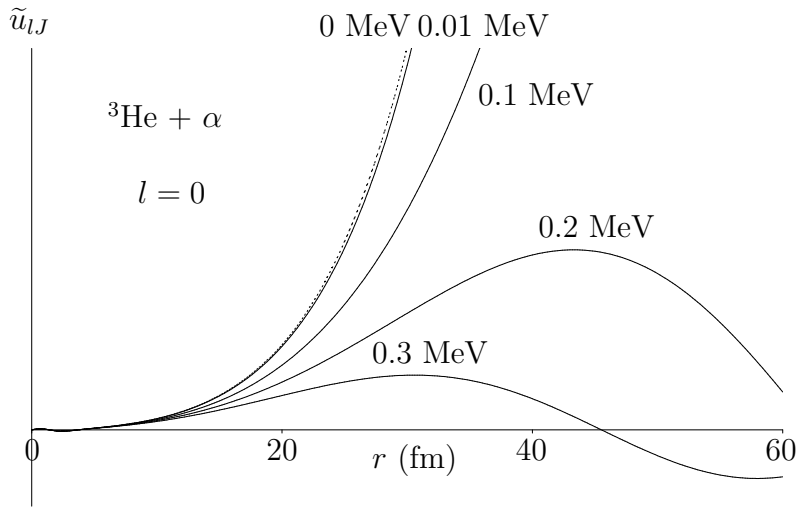

Figure 3. Scaled radial wave functions $\widetilde{u}_{0,1/2}$ of the ^{3}He + α elastic collision at various low energies E. The limit $E \to 0$ is represented as a dotted line.

In practice, this expression may be multiplied by a spectroscopic factor for each component l_f of the final state. The total S factor is obtained by summing over the final states.

Since the physics of low-energy dependences may vary from one initial partial wave to another, it is convenient to focus on some $l_i J_i$ component of $S^{\mathrm{E}\lambda}_{l_f J_f}$. The S factor corresponding to this component is simply denoted as $S(E)$ in the following. Also, spectroscopic factors are not used, except when explicitly mentioned.

The matrix element $I_{l_i J_i}(E)$ is given by the one-dimensional integral

$$I_{l_i J_i}(E) = \int_0^\infty u_{l_f J_f}(r)\, r^\lambda\, \widetilde{u}_{l_i J_i}(E, r)\, dr \tag{42}$$

where $\widetilde{u}_{l_i J_i}$ is defined in Eq. (39). Since $\widetilde{u}_{l_i J_i}$ has a finite limit when E tends towards zero, $I_{l_i J_i}(E)$ and thus $S^{\mathrm{E}\lambda}_{l_f J_f}(E)$ also have finite limits [14].

It is convenient to make use of a function of the phase shift δ_{lJ} defined as

$$D_{lJ}(E) = \frac{2}{\pi}[e^{2\pi\eta} - 1] \tan \delta_{lJ}(E) \tag{43}$$

which also has a finite limit when $E \to 0$ (see Appendix). In the following, I concentrate on very low energies, i.e., on energies verifying

$$e^{-2\pi\eta} \ll 1. \tag{44}$$

This condition is well satisfied for

$$\eta > 1 \quad \text{or} \quad E < E_N. \tag{45}$$

Then, the phase shift δ_{lJ} is very small. With notation (43) and approximation (44), the asymptotic form (40) of the radial wave function becomes for $E < E_N$,

$$\widetilde{u}_{lJ}(E, r) \underset{r\to\infty}{\to} \mathcal{F}_l(E, r) + D_{lJ}(E)\mathcal{G}_l(E, r), \tag{46}$$

which remains finite at $E = 0$.

4.3. Properties of scaled Coulomb functions

Coulomb functions can be described at low energies on the basis of an expansion in powers of $1/\eta^2 = E/E_N$ [15]. Rigorous expressions of such an expansion for F_l and an asymptotic approximation for G_l have been derived by Humblet [16]. Using Eqs. (2.10a) and (4.8a) of Ref. [16], the scaled functions (35) and (36) can be approximated by

$$\mathcal{F}_l(E,r) = \left(\frac{\pi w_l(E)}{1-e^{-2\pi\eta}}\right)^{1/2} r^{1/2}\left[f_0(x) - \frac{1}{12\eta^2}f_1(x) + O\left(\frac{1}{\eta^4}\right)\right] \tag{47}$$

and

$$\mathcal{G}_l(E,r) = \left(\frac{\pi w_l(E)}{1-e^{-2\pi\eta}}\right)^{1/2} r^{1/2}\left[g_0(x) - \frac{1}{12\eta^2}g_1(x) + O\left(\frac{1}{\eta^4}\right)\right] \tag{48}$$

with

$$x = 2(2r/a_N)^{1/2}. \tag{49}$$

The functions $w_l(E)$ read

$$w_l(E) = \prod_{n=0}^{l}\left(1+\frac{n^2}{\eta^2}\right). \tag{50}$$

They are polynomials of degree l of the energy. The first functions f_i read

$$f_0(x) = I_{2l+1}(x), \tag{51}$$

$$f_1(x) = \left(\frac{x}{2}\right)^2\left[3(l+1)I_{2l+3}(x) + \frac{x}{2}I_{2l+4}(x)\right], \tag{52}$$

while the first functions g_i read

$$g_0(x) = K_{2l+1}(x), \tag{53}$$

$$g_1(x) = \left(\frac{x}{2}\right)^2\left[3(l+1)K_{2l+3}(x) - \frac{x}{2}K_{2l+4}(x)\right], \tag{54}$$

where I_n and K_n are modified Bessel, or Hankel, functions [13]. Using notations with an upperscript 0 for functions calculated at zero energy, one deduces from these expressions the limits

$$\mathcal{F}_l^0(r) = \lim_{E\to 0}\mathcal{F}_l(E,r) = (\pi r)^{1/2}f_0(x), \tag{55}$$

$$\mathcal{G}_l^0(r) = \lim_{E\to 0}\mathcal{G}_l(E,r) = (\pi r)^{1/2}g_0(x). \tag{56}$$

Of course, these functions still satisfy the Wronskian relation (37),

$$W\{\mathcal{G}_l^0, \mathcal{F}_l^0\} = \pi/2. \tag{57}$$

The exponential $\exp(-2\pi\eta)$ and all its derivatives tend to zero when E tends to zero. Therefore, the factor $1-\exp(-2\pi\eta)$ in Eq. (47) or (48) behaves as a constant (i.e. unity) in the calculation of a Taylor expansion around $E=0$ and plays no role in this expansion.

One can express with Eqs. (47) and (48) the limits of the first derivatives with respect to energy as

$$\mathcal{F}_l'^0(r) = \frac{(\pi r)^{1/2}}{12E_N}\left[l(l+1)(2l+1)f_0(x) - f_1(x)\right], \tag{58}$$

$$\mathcal{G}_l'^0(r) = \frac{(\pi r)^{1/2}}{12E_N}\left[l(l+1)(2l+1)g_0(x) - g_1(x)\right]. \tag{59}$$

Higher-order derivatives are given in Refs. [17, 18].

4.4. Expansion of $S(E)$ around $E = 0$

All the ingredients needed to perform a Taylor expansion of the S factor near zero energy are now known. Expansion (8) restricted to first order can be rewritten as

$$S(E) \approx S(0)(1 + s_1 E + \ldots). \tag{60}$$

One needs computable expressions of the coefficients. From Eqs. (41) and (42), one immediately obtains

$$S(0) = \tfrac{1}{2}\alpha\hbar c N^{\mathrm{E}\lambda}_{l_i J_i}(|E_{l_f J_f}|/\hbar c)^{2\lambda+1}[I_{l_i J_i}(0)]^2, \tag{61}$$

with the integral

$$I_{l_i J_i}(0) = \int_0^\infty u_{l_f J_f}(r)\, r^\lambda\, \widetilde{u}^0_{l_i J_i}(r)\, dr. \tag{62}$$

The radial wave function $\widetilde{u}^0_{l_i J_i}(r) \equiv \widetilde{u}_{l_i J_i}(0, r)$ at zero energy is a solution of the Schrödinger equation

$$H_{l_i J_i}\widetilde{u}^0_{l_i J_i}(r) = 0. \tag{63}$$

This solution satisfies the boundary conditions

$$\widetilde{u}^0_{l_i J_i}(0) = 0 \tag{64}$$

and

$$\widetilde{u}^0_{l_i J_i}(r) \underset{r\to\infty}{\to} \mathcal{F}^0_{l_i}(r) + D_{l_i J_i}(0)\mathcal{G}^0_{l_i}(r). \tag{65}$$

The normalization of the function $\widetilde{u}^0_{l_i J_i}$ is fixed by Eq. (65). Using Eq. (57), the normalization condition can also be written as

$$W\{\mathcal{G}^0_{l_i}, \widetilde{u}^0_{l_i J_i}\} \underset{r\to\infty}{\to} \pi/2. \tag{66}$$

This Wronskian allows one to properly normalize a numerical solution of Eq. (63) satisfying condition (64). The coefficient $D_{l_i J_i}(0)$ is related to the scattering length by Eq. (A4) and can be calculated with Eq. (A5).

For given $l_i J_i$, the first-order coefficient s_1 in Eq. (60) is obtained by differentiating Eqs. (41) and (42) with respect to E [14], yielding

$$s_1 = \frac{S'(0)}{S(0)} = \frac{2\lambda+1}{|E_{l_f J_f}|} + \frac{2I'_{l_i J_i}(0)}{I_{l_i J_i}(0)}, \tag{67}$$

with the energy derivative of the integral given by

$$I'_{l_i J_i}(0) = \int_0^\infty u_{l_f J_f}(r)\, r^\lambda\, \widetilde{u}'^0_{l_i J_i}(r)\, dr. \tag{68}$$

The first term of Eq. (67) is always positive. Only the second term can explain negative s_1 values.

The energy derivative $\widetilde{u}'^0_{l_i J_i}$ of the radial wave function at zero energy is a solution of the derivative of the Schrödinger equation (21) at the limit $E \to 0$, i.e.,

$$H_{l_i J_i} \widetilde{u}'^0_{l_i J_i}(r) = \widetilde{u}^0_{l_i J_i}(r). \tag{69}$$

The required solution of this inhomogeneous differential equation verifies

$$\widetilde{u}'^0_{l_i J_i}(0) = 0. \tag{70}$$

Its asymptotic form is given by the energy derivative of Eq. (46) at the limit $E \to 0$ as

$$\widetilde{u}'^0_{l_i J_i}(r) \underset{r\to\infty}{\to} \mathcal{F}'^0_{l_i}(r) + D_{l_i J_i}(0)\mathcal{G}'^0_{l_i}(r) + D'_{l_i J_i}(0)\mathcal{G}^0_{l_i}(r), \tag{71}$$

where $\mathcal{F}'^0_{l_i}(r)$ and $\mathcal{G}'^0_{l_i}(r)$ are given by Eqs. (58) and (59), respectively. In this expression, $D'_{l_i J_i}(0)$ is still unknown but this coefficient disappears in the Wronskian limit

$$W\{\mathcal{G}^0_{l_i}, \widetilde{u}'^0_{l_i J_i} - \mathcal{F}'^0_{l_i} - D_{l_i J_i}(0)\mathcal{G}'^0_{l_i}\} \underset{r\to\infty}{\to} 0. \tag{72}$$

The coefficient $D'_{l_i J_i}(0)$ is related to the effective range by Eq. (A7) and can be calculated with Eq. (A8).

A numerical solution of Eq. (69) with the initial condition (70) does not necessarily have the asymptotic behaviour (71) since it may contain an arbitrary component which is solution of the homogeneous equation (63). Subtracting this component to obtain a solution with the correct asymptotic behaviour can easily be performed from the Wronskian limits (72) and (66) (see Ref. [12] for technical details).

4.5. Applications

The ^{3}He(α,γ)^{7}Be reaction is a good example of application of the potential model since the ^{7}Be bound states have an α+^{3}He cluster structure. The dominant multipolarity is E1 ($\lambda = 1$). The spins of the colliding nuclei are $I_1 = 1/2$ and $I_2 = 0$. Hence the channel spin is $I = 1/2$. The quantum numbers of the ^{7}Be ground state are $J_f = 3/2$ and $\pi_f = -1$. The final orbital momentum is thus $l_f = 1$. The capture to the $1/2^-$ first excited state behaves in a similar way. In both cases, the capture can take place from $l_i = 0$ and $l_i = 2$. The capture from the s wave ($J_i = 1/2$) is dominant since this wave has no centrifugal barrier.

Only this case is considered here. The Gaussian potential of Ref. [19] is chosen, like in Ref. [12]. The Bohr radius is $a_N = 4.22$ fm and the Rydberg energy is $E_N = 0.68$ MeV.

Radial wave functions are shown at various energies in Fig. 2. The bound-state wave function exhibits a node near 2 fm due to its orthogonality to a deep unphysical bound state of the potential. With this node, the relative wave function between the clusters is more similar to those obtained from microscopic calculations. Scaled scattering wave functions are presented in Fig. 3.

The integrands in the radial integral (42) are displayed in Fig. 4. They tend to a finite limit (dotted line) thanks to the renormalization with $k^{-1/2}e^{\pi\eta}$. They tend towards this limit from below. One observes that the maximum of the integrand is located near 7.5 fm at very

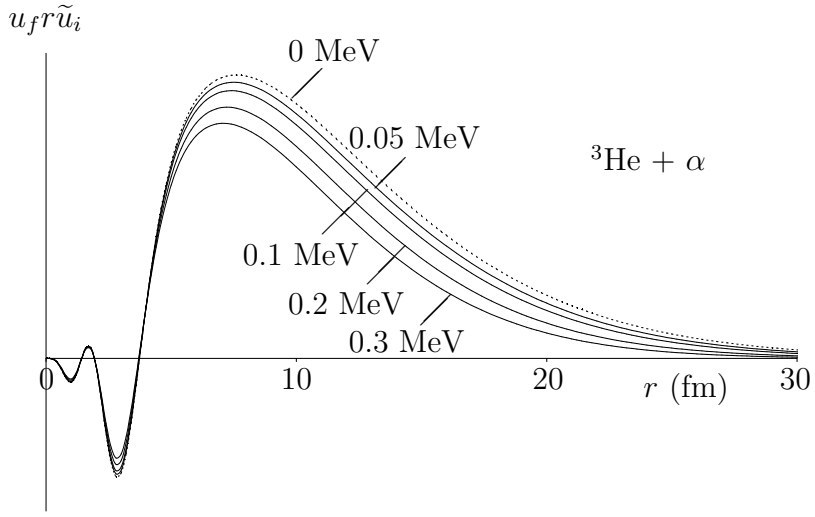

Figure 4. Integrands of the radial E1 integral $I_{0,1/2}(E)$ for the ^{3}He(α,γ)^{7}Be reaction. Notation u_f stands for $u_{1,3/2}(r)$ and $\widetilde{u}_i$ stands for $\widetilde{u}_{0,1/2}(E,r)$. The limit $E \to 0$ is represented as a dotted line.

low energies. The capture thus takes mostly place when the two nuclei do not overlap. The role of the overlap region is restricted to distances below 5 fm. One observes oscillations due to the node near 2 fm of the bound state (see Fig. 2) and the nodes near 1.5 and 3.7 fm of the scattering state (see Fig. 3). The external part of the integrand should not differ much in a more elaborate microscopic model, except possibly for its normalization related to the asymptotic normalization coefficient (ANC). The region below 5 fm is more model dependent but plays a lesser though non negligible role in the value of $I_{0,1/2}(0)$.

The behaviour of the S factor near $E = 0$ is then given by (61) and (67) as [12]

$$S_{g.s.}(0) = 3.2 \times 10^{-4}(1 - 0.88\, E_{\rm MeV})\ {\rm MeV\ b}. \tag{73}$$

For the $1/2^-$ excited state, one obtains

$$S_{1/2^-}(0) = 1.4 \times 10^{-4}(1 - 0.92\, E_{\rm MeV})\ {\rm MeV\ b}. \tag{74}$$

The S factor thus decreases when E increases from $E = 0$. This is the result of two competing effects. The first term in Eq. (67) is positive as always but Fig. 4 shows that the

second term is negative since the area under the curve representing the integrand decreases as E increases. This second term is large enough to give a negative s_1.

The ^{7}Be(p,γ)^{8}B reaction is crucial for the understanding of the solar neutrino emissions since the ^{8}B decay provides most of the high-energy neutrinos from the sun. The spins of the colliding nuclei are $I_1 = 3/2$ and $I_2 = 1/2$. Hence the channel spin is either $I = 1$ or 2. Microscopic calculations indicate that $I = 2$ is dominant in the ground state. The present illustration is restricted to that case for the sake of simplicity. The dominant multipolarity is also E1. The quantum numbers of the ^{8}B ground state are $J_f = 2$ and $\pi_f = +1$. With $I = 2$, the final orbital momentum is thus $l_f = 1$ since the ^{7}Be cluster has a negative parity. The capture can take place from the even $l_i = 0$ and 2. Here also, I only consider the dominant capture from the s wave ($J_i = 2$). The Gaussian potential of Ref. [19] is chosen, like in Ref. [12]. The Bohr radius is $a_N = 8.24$ fm and the Rydberg energy is $E_N = 0.35$ MeV.

The scaled wave functions $\widetilde{u}_{02}$ are presented in Fig. 5 for various low energies and compared with the $E = 0$ limit from Eq. (63). The corresponding integrands in the radial integral (42) are displayed in Fig. 6. They tend from below to a finite limit thanks to the renormalization with $k^{-1/2}e^{\pi\eta}$. They present a maximum around 40 fm. The capture

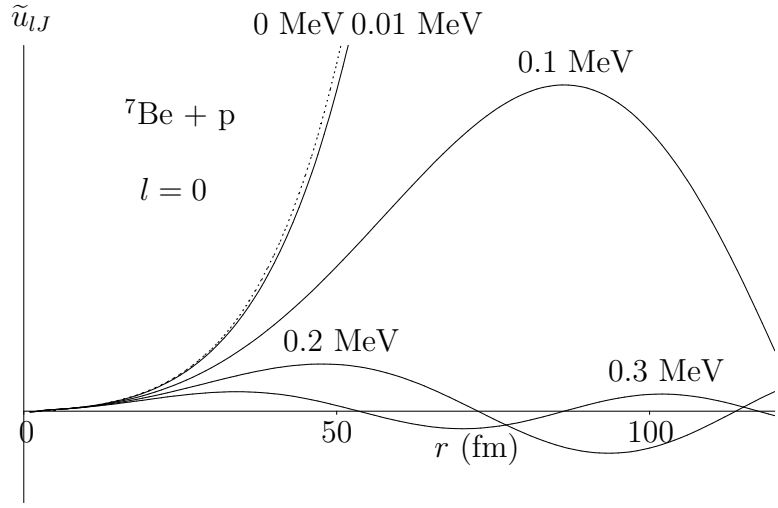

Figure 5. Scaled radial wave functions $\widetilde{u}_{02}$ of the ^{7}Be + p elastic collision. The limit $E \to 0$ is represented as a dotted line.

essentially occurs when the ^{7}Be nucleus and the proton are far away from each other, much farther away than the range of the attractive nuclear interaction. The overlap region is almost totally negligible. The capture cross section at very low energies only depends on asymptotic properties, i.e. the ANC of the bound state and the scattering length a_{02} of the s wave. The dependence of the S factor on these quantities is discussed in the next subsection.

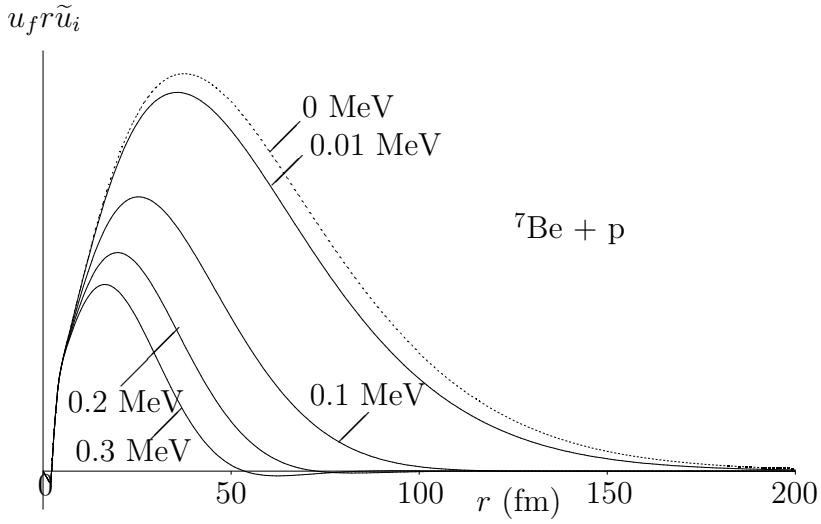

Figure 6. Integrands of the radial E1 integral I_{02} of the ^{7}Be(p,γ)^{8}B reaction. Notation u_f stands for $u_{12}(r)$ and $\widetilde{u}_i$ stands for $\widetilde{u}_{02}(E,r)$. The limit $E \to 0$ is represented as a dotted line.

4.6. External capture approximation

The potential model can sometimes be simplified with the external capture approximation. When the capture essentially occurs at large distances like for ^{7}Be(p,γ)^{8}B, a good approximation can be obtained using only asymptotic expressions [20]. Equation (62) is approximated as [21]

$$I_{l_i J_i}(0) = \int_0^\infty u_{l_f J_f}(r)\, r^\lambda \left[\mathcal{F}^0_{l_i}(r) + D_{l_i J_i}(0)\mathcal{G}^0_{l_i}(r)\right] dr. \tag{75}$$

The approximation made in Eq. (75) is to replace the initial scattering wave function $\widetilde{u}^0_i(r)$ at zero energy by its asymptotic form (46). In this way, one neglects the effect of nodes at short distances in the scattering wave function which simulate the Pauli antisymmetrization in the s wave. The constant $D_{l_i J_i}(0)$ is related to the scattering length $a_{l_i J_i}$ by Eq. (A4) as

$$D_{l_i J_i}(0) = -\frac{4a_{l_i J_i}}{{l_i!}^2 a_N^{2l_i+1}}. \tag{76}$$

The S factor at zero energy explicitly depends on the scattering length (which may not have the dimension of a length) through Eqs. (75) and (76).

Under the same model assumptions, the energy derivative of the radial integral is approximated at zero energy by

$$I'_{l_i J_i}(0) = \int_0^\infty u_{l_f J_f}(r)\, r^\lambda \left[\mathcal{F}'^0_{l_i}(r) + D_{l_i J_i}(0)\mathcal{G}'^0_{l_i}(r) + D'_{l_i J_i}(0)\mathcal{G}^0_{l_i}(r)\right] dr. \tag{77}$$

The energy derivative at zero energy $\widetilde{u}'^0_{l_i J_i}(r)$ of the scattering wave function is also replaced in Eq. (68) by its asymptotic expression (71). The constant $D'_{l_i J_i}(0)$ is related to the scattering length $a_{l_i J_i}$ and to the effective range $r_{l_i J_i}$ by Eq. (A7).

For ^{7}Be(p,γ)^{8}B, the term involving $D'_{l_i J_i}(0)$ is negligible in Eq. (77) [21]. Equation (68) can then be approximated by

$$I'_{l_i J_i}(0) \approx \int_0^\infty u_{l_f J_f}(r)\, r\, [\mathcal{F}'^0_{l_i}(r) + D_{l_i J_i}(0) \mathcal{G}'^0_{l_i}(r)]\, dr. \tag{78}$$

In this approximation, s_1 only depends on the scattering length. Over most of the integration domain, the final bound state wave function is very close to its asymptotic form

$$u_{l_f J_f}(r) \underset{r\to\infty}{\to} C W_{-\eta_b, l_f+1/2}(2k_b r), \tag{79}$$

where $\eta_b = |E_N/E_{l_f J_f}|^{1/2}$, $k_b = (a_N \eta_b)^{-1}$, and W is a Whittaker function [13]. The asymptotic normalization constant C of the final bound state is the main unknown about the nuclear properties of $S(0)$. The initial wave only depends on nuclear effects through the scattering length. The coefficient s_1 is independent of C. The determination of the ratio $S(0)/C^2$ is almost independent of the choice of the final potential. Using $u_{l_f J_f}$ rather than its asymptotic expression (79) has the advantage that the integral automatically converges and that no regularization is needed.

In the evaluation of Eqs. (76) and (78) for ^{7}Be(p,γ)^{8}B, the Woods-Saxon potential established by Barker in Ref. [11] is used, with a slightly modified depth as in Ref. [21] to match the proton separation energy 0.137 keV. Evaluating Eq. (61) with (78) and (79) leads to the expression [21]

$$S(0)/C^2 \approx 35.6(1 - 0.0014 a_{02})\ \text{eV b fm}, \tag{80}$$

where a_{02} is expressed in fm and C in fm$^{-1/2}$. Only the linear term in the s wave scattering length a_{02} is kept. Expression (80) assumes the dominance of external capture. Therefore it should be an accurate approximation of most model calculations of the ^{7}Be(p,γ)^{8}B reaction. The dependence on the scattering length could be significant if this length happened to take large values. However, the measured value of this scattering length does not seem to lead to a correction beyond the percent level [22].

In the same way, a linearized approximation for s_1 can be derived,

$$s_1 \approx -2.47(1 + 0.0072 a_{02})\ \text{MeV}^{-1}. \tag{81}$$

One observes a larger sensitivity to the scattering length, enhanced by a factor of five with respect to Eq. (80). This is due to the strong cancellation between the two terms of expression (67).

In Eq. (81), approximation (78) is used rather than (75), i.e. the effective-range effect is neglected. Varying r_{02} from 0 to the large value 5 fm modifies s_1 by less than half a percent. The effect of the effective range is about an order of magnitude smaller than the effect of the scattering length.

Including d-wave capture leads to the total values [21]

$$S(0)/C^2 \approx 38.0(1 - 0.0013 a_{02})\ \text{eV b fm} \tag{82}$$

and

$$s_1 \approx -1.81(1 + 0.0087 a_{02})\ \mathrm{MeV}^{-1}. \tag{83}$$

The dependence on the scattering length is thus weak.

Estimates of the dependence on the scattering length for other systems where the external-capture approximation is valid for some states such as ^{12}C$(\alpha,\gamma)^{16}$O or ^{16}O(p,$\gamma)^{17}$F have shown an even weaker dependence on the scattering length.

4.7. Interpretation of external capture

External capture can be interpreted with the help of the WKB approximation [20, 4]. The scaled Coulomb functions can be approximated as

$$\mathcal{F}_l(E,r) \approx \frac{1}{2}\left(\frac{1}{2}a_N r\right)^{1/4} e^{\varphi_l(k,r)} \tag{84}$$

and

$$\mathcal{G}_l(E,r) \approx \frac{\pi}{2}\left(\frac{1}{2}a_N r\right)^{1/4} e^{-\varphi_l(k,r)} \tag{85}$$

where

$$\varphi_l(k,r) = \left(\frac{2r}{a_N}\right)^{1/2}\left(2 - \frac{l^2 a_N}{r} - \frac{1}{6}a_N k^2 r\right) \tag{86}$$

under the condition

$$a_N < r < \eta^2 a_N. \tag{87}$$

The WKB approximation is thus valid only for $E < E_N$. However, qualitatively, it can have a larger range of validity. Hence the asymptotic form (40) of a scattering wave function can be approximated as

$$\widetilde{u}_{lJ}(E,r) \underset{r\to\infty}{\to} \frac{1}{2}\left(\frac{1}{2}a_N r\right)^{1/4}\left[e^{\varphi_l(k,r)} - \pi\frac{a_{lJ}}{l!^2 a_N^{2l+1}} e^{-\varphi_l(k,r)}\right]. \tag{88}$$

One observes that the energy dependences of the two exponentials are opposite.

Let us apply this to the ^{7}Be+p capture in the s wave. The scattering length is close to the value of a_N. At the low energies where the WKB approximation is valid, the first term in (88) is much larger than the second one. More generally, $\mathcal{F}_0$ is much larger than $\pi(a_{02}/a_N)\mathcal{G}_0$ at these energies. Hence the scattering wave function is well approximated asymptotically by the first term of the WKB approximation (88). The energy dependence in (86) explains the decrease of the scattering wave functions in Fig. 5 when the energy increases from zero and thus the decrease of the integrand displayed in Fig. 6. Differentiating $\exp[\varphi_l(k,r)]$ with respect to E and using the mean-value theorem leads to

$$s_1 \approx \frac{2\lambda+1}{|E_{l_f J_f}|} - \frac{\sqrt{2}}{3E_N}\left(\frac{\bar{r}}{a_N}\right)^{3/2} \tag{89}$$

where $\bar{r}$ is the location of the maximum of $u_{l_f J_f}(r)\, r^{\lambda+3/2}\, \widetilde{u}^0_{l_i J_i}(r)$ [4]. The main merit of this rough approximation is to show that s_1 results from a subtraction of two quantities with very different physical contents.

For the α+^{3}He capture, the scattering length is larger [12, 7], i.e. approximately $9a_N$, but the second exponential in Eq. (88) remains essentially negligible. Hence the scaled scattering wave functions in Fig. 3 and the integrands in Fig. 4 decrease at large distances when the energy increases from zero. The WKB approximation (confirmed by numerical values of the Coulomb functions) offers a simple qualitative explanation of the origin of negative s_1 values when external capture dominates.

The asymptotic form (79) of a bound-state wave function becomes at very large distances

$$u_{lJ}(r) \propto r^{-\eta_b} e^{-k_b r} \tag{90}$$

for $r > \eta_b^2 a_N$ or

$$u_{lJ}(r) \propto r^{1/4} e^{-(2r/a_N)^{1/2}(2-l^2 a_N/2r + a_N k^2 r/6)} \tag{91}$$

for $a_N < r < \eta_b^2 a_N$. The location of the maximum of the integrand in Eq. (75) is then roughly given either by [4]

$$r_m \approx \frac{1}{2}\eta_b a_N \left[\eta_b^{1/2} + \left(2\lambda + \tfrac{1}{2} - \eta_b\right)^{1/2}\right]^2 \tag{92}$$

or by

$$r_m \approx a_N^{1/3}[(2\lambda+1) Z_1 Z_2 \alpha/\sqrt{2}k_\gamma]^{2/3}. \tag{93}$$

These rough estimates of the location of the maximum can give an idea of the validity of the external-capture approximation. The radius $\bar{r}$ appearing in Eq. (89) can be estimated with (92) or (93) by replacing λ by $\lambda + 3/2$.

5. Proton-proton weak capture

Although not a radiative-capture process, the proton-proton weak capture behaves in a very similar way. In a proton-proton collision, the weak interaction can transform a proton into a neutron to form a deuteron with emission of a positron and a neutrino. This reaction has the small Q value 0.42 MeV. The deuteron quantum numbers are $J_f = 1$ and $\pi_f = +1$. With an intrinsic spin $S_f = 1$, the orbital momentum l_f is 0 or 2. The identity of the protons imposes $l_i + S_i$ even. The parity does not change in this Gamow-Teller transition. The initial orbital momentum is thus $l_i = 0$ or 2 with $S_i = 0$.

Here I consider a very simplified model of this capture, i.e. the tensor force is neglected and the nucleon-nucleon interaction is approximated by the purely central Minnesota potential [23]. The deuteron wave function is then limited to the s wave. After integration of the leptonic part of the matrix elements, the weak-capture cross section reduces under these approximations to the simple Gamow-Teller expression

$$\sigma(E) = \frac{6 m_e c^2}{\pi^2 \hbar v k^2}\, G_\beta^2 \lambda^2 f(E+Q) \left[\int_0^\infty u_{01}^{\rm d}(r) u_{00}^{\rm pp}(E,r) dr\right]^2, \tag{94}$$

where m_e is the electron mass, $G_\beta \approx 3 \times 10^{-12}$ is the dimensionless β-decay constant, $\lambda \approx -1.25$ is the Gamow-Teller to Fermi ratio, $f(E)$ is the Fermi integral and $u_{01}^{\rm d}$ is the deuteron radial wave function. The scattering wave function $u_{00}^{\rm pp}$ is normalized as

$$u_{00}^{\rm pp}(E,r) \underset{r\to\infty}{\to} \cos\delta_{00}(E)F_0(\eta,kr) + \sin\delta_{00}(E)G_0(\eta,kr) \tag{95}$$

and thus tends to zero at any given distance when $E \to 0$. It is thus convenient to introduce as before

$$\widetilde{u}_{00}^{\rm pp}(E,r) = k^{-1/2}e^{\pi\eta}u_{00}^{\rm pp}(E,r). \tag{96}$$

These functions are displayed in Fig. 7 for various small energies and for $E = 0$. For comparison, the deuteron wave function $u_{01}^{\rm d}$ is also represented. Because of the small binding energy, it decreases slowly with r.

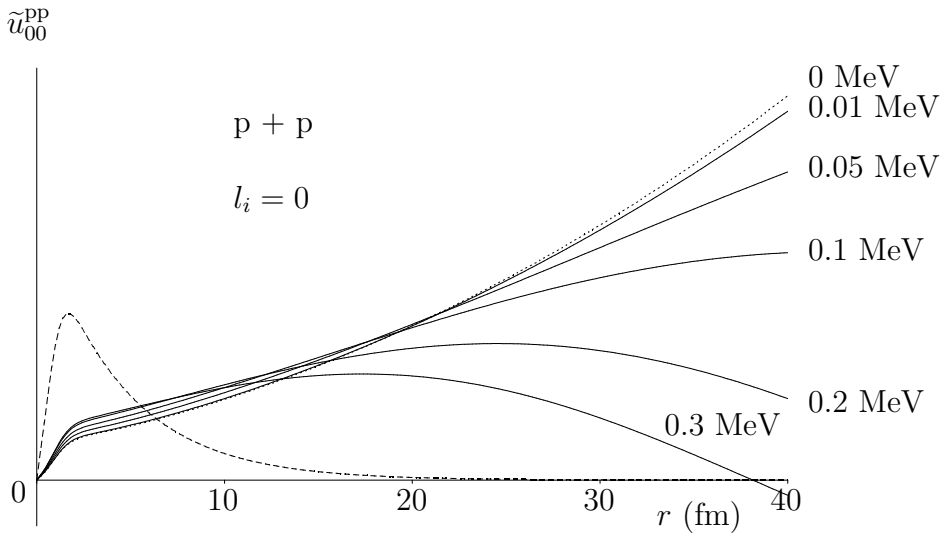

Figure 7. Scaled radial s wave functions $\widetilde{u}_{00}^{\rm pp}$ of the elastic p + p collision for different energies E. The limit $E \to 0$ is represented as a dotted line. The deuteron wave function $u_{01}^{\rm d}$ ($\times 20$) is displayed as a dashed line.

The S factor is then simply given by

$$S(E) = \frac{3}{\pi^2}\, m_e c^2 G_\beta^2 \lambda^2 f(E+Q)[I(E)]^2 \tag{97}$$

where

$$I(E) = \int_0^\infty u_{01}^{\rm d}(r)\widetilde{u}_{00}^{\rm pp}(E,r)dr. \tag{98}$$

The integrand is presented in Fig. 8. One observes that the area under the curve increases with E. The Fermi integral $f(Q+E)$ also increases with E as the phase space enlarges. Hence, one expects the S factor to increase with E near $E = 0$.

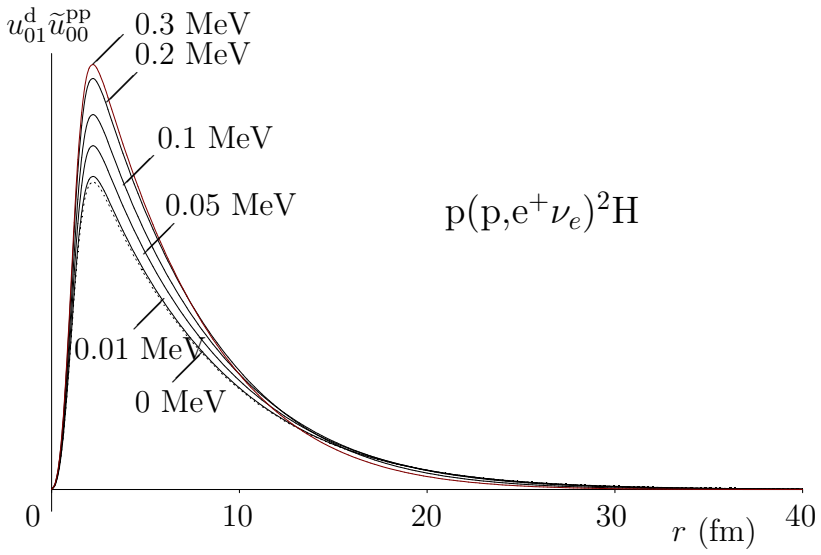

Figure 8. Integrands of radial integrals $I(E)$ of the p(p,e$^+\nu_e$)^{2}H reaction for different energies E. The limit $E \to 0$ is represented as a dotted line.

At zero energy, one obtains in the same way as before

$$S(0) = \frac{3}{\pi^2}\, m_e c^2 G_\beta^2 \lambda^2 f(Q)[I(0)]^2 \tag{99}$$

calculated with the solution of Eq. (63) and

$$s_1 = \frac{f'(Q)}{f(Q)} + \frac{2I'(0)}{I(0)} \tag{100}$$

involving the solution of Eq. (69). After a multiplication by 0.94 to compensate the absence of d component in the deuteron wave function, the low-energy S factor is given by

$$S(E) \approx 4.0 \times 10^{-25}(1 + 11.4E_{\mathrm{MeV}})\ \mathrm{MeV\ b}. \tag{101}$$

The slope coefficient s_1 should be rather accurate in spite of the simplicity of the approximation. It agrees with various other estimates [24]. An accurate determination of the value of $S(0)$ requires a more realistic interaction and taking account of exchange currents [24].

6. Neutron radiative capture

6.1. Expansion of σv

The non-resonant behaviour of neutron-capture cross sections at low energy is well understood theoretically. At low relative energies E, as explained below, the product σv of the

neutron-capture cross section $\sigma(E)$ to a given bound state and of the initial relative velocity v can be approximated by a Taylor expansion truncated at first order [25],

$$\sigma v = S_0 E^{l_i}(1 + s_1 E + \ldots), \tag{102}$$

where l_i is the smallest relevant orbital momentum of the initial scattering state.

In practice, a multipole transition starting from $l_i = 0$ is always possible to some bound state but it may be strongly hindered if its multipolarity (electric or magnetic) is high. Hence, at sufficiently low energies, one always has

$$\sigma v = S_0(1 + s_1 E + \ldots), \tag{103}$$

but the energy range where this expression is valid may not be accessible to experiment or interesting for astrophysics. It can be far below the thermal energy.

Let me now justify Eq. (102) in the potential model. A neutron is captured by a nucleus with mass A_1 and charge $Z_1 e$ from the initial partial wave $l_i J_i$. The cross section (27) multiplied by the relative velocity v is given in the potential model by

$$\sigma v = \alpha c N^{\mathrm{E}\lambda}_{l_i J_i} k_\gamma^{2\lambda+1} k^{2l_i} [I(E)]^2, \tag{104}$$

where $N^{\mathrm{E}\lambda}_{l_i J_i}$ is given by (29) for $A_2 = 1$ and $Z_2 = 0$, i.e. $Z^{\mathrm{E}\lambda}_{\mathrm{eff}} = Z_1(-1/A)^\lambda$. The integral $I(E)$ is still given by Eq. (42) in which the scaled radial function $\widetilde{u}_{l_i J_i}$ possesses the asymptotic behaviour

$$\widetilde{u}_{lJ}(E,r) \underset{r\to\infty}{\to} \cos\delta_{lJ}(E)\left[\mathcal{F}_l(E,r) + D_{lJ}(E)\mathcal{G}_l(E,r)\right], \tag{105}$$

where the first factor can not be approximated by unity like in Eq. (46) and the definitions of the scaled functions $\mathcal{F}_l$ and $\mathcal{G}_l$ are different. They are defined as [17, 25]

$$\mathcal{F}_l(E,r) = k^{-l} r j_l(kr) \tag{106}$$

and

$$\mathcal{G}_l(E,r) = k^{l+1} r n_l(kr) \tag{107}$$

where j_l and $n_l = -y_l$ are spherical Bessel functions [13]. The coefficient of $\mathcal{G}_l$ in Eq. (46) is defined as

$$D_{lJ}(E) = k^{-2l-1}\tan\delta_{lJ}(E). \tag{108}$$

Notice that while the asymptotic behaviour (105) in the neutral case has a mathematical form similar to (46) in the charged case, the dimensions of $\mathcal{F}_l$, $\mathcal{G}_l$ and D_{lJ} are different.

The Taylor expansion (102) can now be understood. The functions $\mathcal{F}_{l_i}$ and $\mathcal{G}_{l_i}$ and hence the scaled scattering function $\widetilde{u}_{l_i J_i}$ with the asymptotic behaviour (46) have a finite non-zero limit for $E \to 0$. The same property is true for $I(E)$. The factor E^{l_i} in Eq. (102) thus comes from the factor k^{2l_i} in expression (104) of σv. The coefficients S_0 and s_1 of the Taylor expansion (102) can be derived by a simple direct calculation at energy zero [25]. Notice that S_0 as defined here [26] is slightly different from the definition in Ref. [25]. It differs from $\mathcal{S}_0$ of Ref. [25] by a factor $(2\mu/\hbar^2)^{l_i}$.

The limit of σv for $E \to 0$ is given by

$$S_0 = \alpha c N^{\mathrm{E}\lambda}_{l_i J_i} (|E_{l_f J_f}|/\hbar c)^{2\lambda+1} (2\mu/\hbar^2)^{l_i} [I_{l_i J_i}(0)]^2. \tag{109}$$

The integral $I(0)$ is given by Eq. (62) but with a different definition for the normalization of $\widetilde{u}^0_{l_i J_i}$. Since Eq. (64) does not fix the normalization, function $\widetilde{u}^0_{l_i J_i}$ must be normalized by imposing the condition

$$W\{\mathcal{G}^0_{l_i}, \widetilde{u}^0_{l_i J_i}\}_{r\to\infty} \to 1, \tag{110}$$

where the limits of the irregular spherical Bessel functions are [17]

$$\mathcal{G}^0_0 = 1, \;\; \mathcal{G}^0_1 = r^{-1}, \;\; \ldots \tag{111}$$

The limits of the regular spherical Bessel functions are

$$\mathcal{F}^0_0 = r, \;\; \mathcal{F}^0_1 = r^2/3, \;\; \ldots \tag{112}$$

General expressions for $\mathcal{F}^0_l$ and $\mathcal{G}^0_l$ and their energy derivatives can be found in Ref. [17].

The coefficient s_1 in expansion (102) reads

$$s_1 = \frac{2\lambda+1}{|E_{l_f J_f}|} + \frac{2I'_{l_i J_i}(0)}{I_{l_i J_i}(0)} - \delta_{l_i 0} \frac{2\mu a^2_{0J_i}}{\hbar^2}, \tag{113}$$

where a_{0J_i} is the s-wave scattering length. Notice the occurrence of an additional term for $l_i = 0$ coming from the factor $\cos\delta_{l_i J_i}(E)$ in Eq. (105) and the effective-range expansion (A1) of the phase shift. The integral $I'_{l_i J_i}(0)$ is given by Eq. (68). The energy derivative of the radial wave function at zero energy $\widetilde{u}'^0_{l_i J_i}$ is a solution of the derivative (69) of the Schrödinger equation at the limit $E \to 0$. Since solutions vanishing at the origin are not uniquely fixed by this equation, one imposes the condition

$$W\{\mathcal{G}^0_{l_i}, \widetilde{u}'^0_{l_i J_i} - \mathcal{F}'^0_{l_i} + a_{l_i J_i} \mathcal{G}'^0_{l_i})\}_{r\to\infty} \to 0, \tag{114}$$

where $a_{l_i J_i}$ is the scattering length of partial wave $l_i J_i$ and

$$\mathcal{F}'^0_0 = -r^3/3, \;\; \mathcal{F}'^0_1 = -r^4/15, \ldots \tag{115}$$

$$\mathcal{G}'^0_0 = -r^2, \;\; \mathcal{G}'^0_1 = r, \ldots \tag{116}$$

The scattering length can be accurately calculated with Eqs. (A3) and (A5) of the Appendix.

6.2. Applications

The ^{12}C(n,γ)^{13}C capture reaction is well studied experimentally. Data exist for the capture towards the four bound states of ^{13}C (see references in Ref. [25]). Most references use the neutron energy E_n rather than the energy E of the relative motion employed here. This reaction is described in the potential model with the Woods-Saxon potentials given in Table I of Ref. [25]. At very low energies, the capture proceeds dominantly towards the $1/2^-$ ground state and the $3/2^-$ second excited state providing

$$\sigma v \approx 2.6 \times 10^{-5} (1 - 0.74 E_{\mathrm{MeV}} + 23.5 E^2_{\mathrm{MeV}}) \text{ mb } c. \tag{117}$$

in agreement with Eq. (103) since E1 capture is possible from the s wave. Notice however the large coefficient of $E^2_{\rm MeV}$ mostly coming from d-wave capture. The potential-model results are multiplied by spectroscopic factors (0.88 for the ground state and 0.15 for the $3/2^-$ state) derived by comparing the model with thermal capture cross sections (see Ref. [25] for details and in particular Table II of that reference).

The capture from the p wave to the $1/2^+$ excited state plays however a crucial role above 1 keV. The integrand for the $p1/2$ to $s1/2$ transition is displayed in Fig. 9. One observes that the capture takes place at rather large distances since the maximum is beyond 10 fm. The slow decrease of the wave function of the weakly bound $s1/2$ state leads to a large integral. The area below the curves decreases rather fast with increasing energy. One can expect the same behaviour for σv. The $1/2^+$ state is a good single-particle state. Its

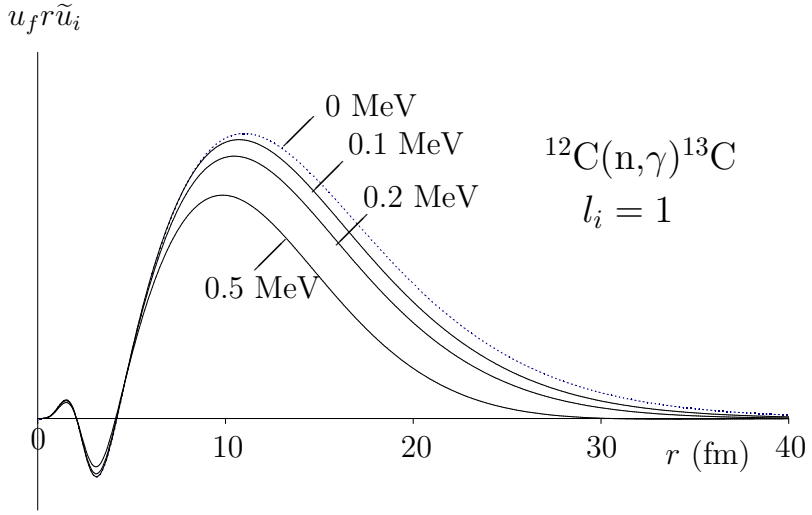

Figure 9. Product $u_f r\widetilde{u}_i$ for the $p1/2$ to $s1/2$ transition for the ^{12}C(n,γ)^{13}C reaction. Notation u_f stands for $u_{0,1/2}$ and $\widetilde{u}_i$ stands for $\widetilde{u}_{1,1/2}$. The limit $E \to 0$ is represented as a dotted line.

spectroscopic factor is 0.95. The product σv follows Eq. (102) with $l_i = 1$ and is given by

$$\sigma v \approx 2.2 \times 10^{-3} E_{\rm MeV}(1 - 0.85 E_{\rm MeV})\ {\rm mb}\ c. \tag{118}$$

The calculated capture cross sections to the various bound states agree fairly well with the available data between 20 and 500 keV. When summing the contributions (117) and (118), one obtains

$$\sigma v \approx 2.6 \times 10^{-5}(1 + 88 E_{\rm MeV} - 50 E^2_{\rm MeV})\ {\rm mb}\ c \tag{119}$$

which provides a good parametrization of all sub-MeV experimental cross sections [25]. The famous $1/v$ behaviour of the neutron-capture cross section is valid below 1 keV. But, as displayed in Fig. 10, it is not followed above that energy as observed in experiments [27]. This should not be considered as a surprise. Above 1 keV, the p wave capture to the $1/2^+$

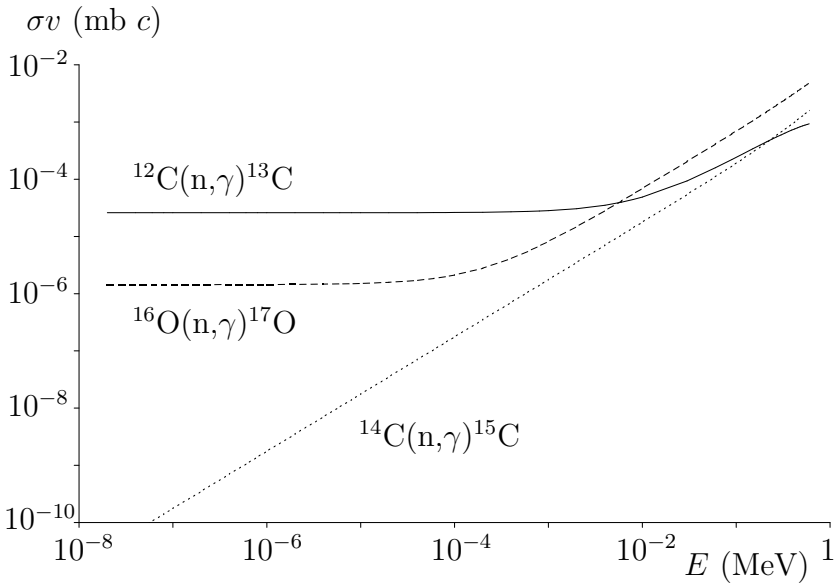

Figure 10. Product σv at low energies for the ^{12}C(n,γ)^{13}C (full line), ^{14}C(n,γ)^{15}C (dotted line) and ^{16}O(n,γ)^{17}O (dashed line) reactions.

excited state becomes dominant and Eq. (103) is replaced by Eq. (102) with $l_i = 1$. Such an effect is made possible by the occurrence of states of both parities in the bound spectrum.

For the ^{14}C(n,γ)^{15}C E1 capture, the reaction can proceed only from the p wave since both ^{15}C bound states have positive parity. The single-particle nature of these states allows using the potential model with good accuracy. No spectroscopic factors are used. The Woods-Saxon potential is given in Table III of Ref. [26]. The main contribution comes from the capture to the $1/2^+$ ground state, the $5/2^+$ excited state accounting only for a few percents. The total σv at low energy is given by

$$\sigma v \approx 1.76 \times 10^{-3} E_{\rm MeV}(1 - 0.85 E_{\rm MeV}) \text{ mb } c. \tag{120}$$

Notice the additional factor $E_{\rm MeV}$ due to the initial p wave. This parametrization agrees with the few existing data points between 20 and 700 keV [26]. This behaviour is presented in Fig. 10 but one should keep in mind that M1 transitions (which vanish exactly in the potential model but are not forbidden) should level off the curve somewhere at very low energies. This flat part of the curve can in principle be deduced from measurements of the capture cross section at thermal energies. However, one only knows the upper bound 1 μb for the thermal capture cross section. The $1/v$ behaviour should be valid somewhere below 1 eV ($\sigma v < 7 \times 10^{-9}$ mb c).

The ^{16}O(n,γ)^{17}O capture reaction has been observed towards the three lowest ^{17}O bound states (see references in Ref. [26]). The Woods-Saxon potential is given in Table V of Ref. [26]. The main contributions come from the captures to the $1/2^+$ first excited state and the $5/2^+$ ground state. These transitions correspond to p-wave capture. Without spectroscopic factors, they lead to

$$\sigma v \approx 6.72 \times 10^{-3} E_{\rm MeV}(1 + 0.32 E_{\rm MeV}) \text{ mb } c. \tag{121}$$

Contrary to the ^{14}C(n,γ)^{15}C case, the thermal capture cross section has been measured. It allows evaluating approximately the cross sections for the capture processes dominant at very low energies, i.e. the global effect of the E1 capture to the $3/2^-$ excited state and of the M1 capture to the $1/2^+$ state. These captures both start from the s wave and thus follow Eq. (103). With an approximate treatment of these contributions fitting the thermal cross section, the total σv can be parametrized as [26]

$$\sigma v \approx 1.44 \times 10^{-6}(1 + 4660 E_{\rm MeV} + 1480 E_{\rm MeV}^2)\ {\rm mb}\ c. \tag{122}$$

As shown in in Fig. 10, the $1/v$ behaviour is valid below about 0.1 keV but a stronger energy dependence starts to dominate above that energy. Parametrization (122) agrees with the few existing data between 19 and 260 keV, and of course with the fitted thermal cross section [26].

7. R-matrix descriptions

The previous studies are based on the potential model, where the internal structure of the colliding nuclei and the effects of antisymmetrization are neglected. This is a good approximation in some cases but many reactions require a more elaborate treatment. Nevertheless the principle of the above analysis of very low energies remains valid in microscopic and *ab initio* models. The renormalization of the Coulomb functions remains necessary at large distances and imposes a modification of the wave functions at shorter distances where the microscopic structure plays its role. This can easily be taken into account in the framework of the R-matrix theory [6].

The R-matrix method is useful both for microscopic and non microscopic descriptions of radiative capture as well as for phenomenological fits of experimental data [6]. In this method, the configuration space is separated into two parts. This separation is characterized by a parameter, the channel radius a. In the internal region, the Schrödinger equation is solved, with full account of antisymmetrization in microscopic models. In the external region, the wave functions are approximated by their asymptotic form, i.e. a product of the internal functions of the colliding nuclei and the wave function of their relative motion with appropriate angular momentum couplings; antisymmetrization effects and the residual nuclear interaction between the nuclei are neglected. When the channel radius a is large enough, the results are insensitive to its value. This procedure is also valid, and much simpler, to calculate cross sections in the potential model, even if this potential is non local [9, 28]. In all cases, the treatment in the external region is similar to the treatment of asymptotic properties presented in previous sections.

A Taylor expansion of $S(E)$ can be derived in this general framework. The S factor can be derived from Eq. (18) as [29]

$$S(E) \propto \sum_{\sigma\lambda} k_\gamma^{2\lambda+1} \sum_{l_i I J_i} \left| M_{\rm int}(E) + M_{\rm ext}(E) \right|^2 . \tag{123}$$

In this expression, the internal transition matrix element $M_{\rm int}(E)$ is calculated over the internal region, e.g. with antisymmetric wave functions in microscopic models. It can be expressed as a function of poles and reduced widths in a typical R-matrix way. In potential

and microscopic models, the poles and reduced widths are obtained from solutions of the Bloch-Schrödinger equation [6, 28]. In phenomenological models, they are obtained from fits to experiments.

The external transition matrix element $M_{\rm ext}(E)$ is calculated along the ways explained in previous sections. It involves an integral very similar to Eq. (75) but with a lower limit a of integration in place of 0. When internal capture is negligible, the model is equivalent to the extranuclear-capture model described above. When external capture is negligible, only $M_{\rm int}(E)$ must be taken into account. An example of this case can be found in Ref. [30].

The S factor at energy zero and coefficient s_1 are directly obtained from Eq. (123). Both parts $M_{\rm int}(E)$ and $M_{\rm ext}(E)$ of the matrix element have a finite non-zero limit when E tends to zero. The technical details may be heavy and are not presented here. This approach is of course also valid for the coefficients of a Taylor expansion of σv in the neutral case.

8. Conclusion

The physics of radiative capture can be analyzed down to energy zero in any model, microscopic or non-microscopic. To this end, a specific normalization of the scattering wave functions is necessary, inspired by a scaling of the Coulomb functions that leads to finite non-zero limits for $E = 0$. The S factor at zero energy, the slope of its energy dependence near the origin and higher coefficients of its Taylor expansion, if necessary, can be calculated accurately. An accurate theoretical description of this low-energy behaviour is important as cross sections in this energy domain are in general not accessible to experiment for the radiative capture of charged particles.

In the potential model, simple pictures of the integrands of the radial matrix elements allow a qualitative understanding of the properties of the S factor at very low energies. Some of those properties can be understood with the extranuclear capture model. The same kind of analysis can be performed for the charged-particle and neutron radiative captures, with different normalizations of the scattering wave functions. It also applies to the proton-proton weak capture.

Microscopic models, and among them *ab initio* models, can make use of the present developments generalized in the context of the R-matrix theory.

Acknowledgments

This text presents research results of the interuniversity attraction pole programme P7/12 initiated by the Belgian-state Federal Services for Scientific, Technical and Cultural Affairs.

Appendix: Effective-range expansion

In this Appendix, the scattering length and effective range are derived from solutions of the Schrödinger equation (63) and its energy detivative (69) at zero energy [12, 17]. For an

arbitrary partial wave, the effective-range expansion is given in the neutral case by [31, 32]

$$\frac{1}{D_{lJ}(E)} = -\frac{1}{a_{lJ}} + \frac{1}{2} r_{lJ} k^2 + O(k^4), \tag{A1}$$

where D_{lJ} is defined in Eq. (108), and in the charged case by [33, 34]

$$\frac{2w_l(E)}{l!^2 a_N^{2l+1}} \left[\frac{2}{D_{lJ}(E)} + h(\eta) \right] = -\frac{1}{a_{lJ}} + \frac{1}{2} r_{lJ} k^2 + O(k^4), \tag{A2}$$

where D_{lJ} is defined in Eq. (43) and notations (5) and (50) are used. The low-energy properties of function $h(\eta)$ [33, 34] are described in Refs. [12, 17].

By taking the limit $E \to 0$ of both sides of Eqs. (A1) and (A2), the scattering length reads in the neutral case [25]

$$a_{lJ} = -D_{lJ}(0) \tag{A3}$$

and in the charged case [12]

$$a_{lJ} = -\frac{l!^2 a_N^{2l+1}}{4} D_{lJ}(0), \tag{A4}$$

where $D_{lJ}(0)$ is easily calculated with

$$D_{lJ}(0) = -\frac{2\mu}{\hbar^2} \int_0^\infty \mathcal{F}_l^0(r) V_{\rm sr}(r) \widetilde{u}_{lJ}^0(r) dr. \tag{A5}$$

In this integral, $V_{\rm sr}(r) = V_{\rm N}^{lJ}(r) + V_{\rm C}(r) - Z_1 Z_2 e^2/r$ is the short-range part of the potential. Equations (A3), (A4) and (A5) provide a simple and accurate way of calculating the scattering length.

The value of the effective range is given in the neutral case by

$$r_{lJ} = -\frac{\hbar^2}{\mu a_{lJ}^2} D'_{lJ}(0) \tag{A6}$$

and in the charged case by

$$r_{lJ} = \frac{1}{3l!^2 a_N^{2l-1}} \left[1 + \frac{4l(l+1)(2l+1)}{D_{lJ}(0)} - \frac{24 E_N D'_{lJ}(0)}{D_{lJ}(0)^2} \right], \tag{A7}$$

where

$$D'_{lJ}(0) = -\frac{2\mu}{\hbar^2} \int_0^\infty V_{\rm sr}(r) \left[\mathcal{F}_l^0(r) \widetilde{u}_{lJ}'^0(r) + \mathcal{F}_l'^0(r) \widetilde{u}_{lJ}^0(r) \right] dr. \tag{A8}$$

Accurate values of the effective range r_{lJ} can be deduced from Eqs. (A6) or (A7) since the integrand in Eq. (A8) is short-ranged. The functions $\mathcal{F}_l^0$ and $\mathcal{G}_l^0$ and the derivatives with respect to energy are calculated with (111), (112), (115) and (116) in the neutral case and with (55), (56), (58) and (59) in the charged case.

For $l = 0$, this approach provides an alternative to the famous Schwinger-Bethe formula [31, 32], which reads in the present notation for the charged case [12],

$$r_{0J} = \frac{16}{\pi a_N D_{0J}(0)^2} \int_0^\infty \left\{ \left[\mathcal{F}_0^0(r) + D_{0J}(0) \mathcal{G}_0^0(r) \right]^2 - \left[\widetilde{u}_{0J}^0(r) \right]^2 \right\} dr. \qquad \text{(A9)}$$

In the neutral case, the coefficient in front of the integral is $2/D_{0J}(0)^2$. Equations (A6) and (A7) converge much faster than Eq. (A9) and remain valid for $l > 0$.

The next term of the effective-range expansion is given in Ref. [17]. Higher orders are considered in Ref. [18].

References

[1] Fowler, W. A.; Caughlan, G. R.; Zimmerman, B. A. *Ann. Rev. Astron. Astrophys.* 1967, *5*, 525.

[2] Fowler, W. A.; Caughlan, G. R.; Zimmerman, B. A. *Ann. Rev. Astron. Astrophys.* 1975, *13*, 69.

[3] Angulo, C.; Arnould, M.; Rayet, M.; Descouvemont, P.; Baye, D.; Leclercq-Willain, C.; Coc, A.; Barhoumi, S.; Auger, P.; Rolfs, C.; Kunz, R.; Hammer, J. W.; Mayer, A.; Paradellis, T.; Kossionides, S.; Chronidou, C.; Spyrou, K.; Degl'Innocenti, S.; Fiorentini, G.; Ricci, B.; Zavatarelli, S.; Providencia, C.; Wolters, H.; Soares, J.; Grama, C.; Rahighi, J.; Shotter, A.; Lamehi-Rachti, M. *Nucl. Phys. A* 1999, *656*, 3.

[4] Baye, D.; Descouvemont, P. *Ann. Phys.* 1985, *165*, 115.

[5] Baye, D.; Descouvemont, P. *Nucl. Phys. A* 1983, *407*, 77.

[6] Descouvemont, P.; Baye, D. *Rep. Prog. Phys.* 2010, *73*, 036301.

[7] Kamouni, R.; Baye, D. *Nucl. Phys. A* 2007, *791*, 68.

[8] Neff, T. *Phys. Rev. Lett.* 2011, *106*, 042502.

[9] Navrátil, P.; Roth, R.; Quaglioni, S. *Phys. Lett. B* 2011, *704*, 379.

[10] Tombrello, T. A. *Nucl. Phys.* 1965, *71*, 459.

[11] Barker, F. C. *Aust. J. Phys.* 1980, *33*, 177.

[12] Baye, D.; Brainis, E. *Phys. Rev. C* 2000, *61*, 025801.

[13] Abramowitz, M.; Stegun, I. A. *Handbook of Mathematical Functions* (Dover: New York), 1965.

[14] Baye, D.; Descouvemont, P.; Hesse, M. *Phys. Rev. C* 1998, *58*, 545.

[15] Hull Jr., M. H.; Breit, G. *Encyclopedia of Physics*; Flügge, S.; Ed.; Vol. XLI/1 (Springer: Berlin), 1959, p. 408.

[16] Humblet, J. *J. Math. Phys.* 1985, *26*, 656.

[17] Baye, D.; Hesse, M.; Kamouni, R. *Phys. Rev. C* 2000, *63*, 014605.

[18] Ramirez Suarez, O.; Sparenberg, J.-M. *submitted*.

[19] Buck, B.; Baldock, R. A.; Rubio, J. A. *J. Phys. G* 1985, *11*, L11.

[20] Christy, R. F.; Duck, I. *Nucl. Phys.* 1961, *24*, 89.

[21] Baye, D. *Phys. Rev. C* 2000, *62*, 065803.

[22] Angulo, C.; Azzouz, M.; Descouvemont, P.; Tabacaru, G.; Baye, D.; Cogneau, M.; Couder, M.; Davinson, T.; Di Pietro, A.; Figuera, P.; Gaelens, M.; Leleux, P.; Loiselet, M.; Ninane, A.; de Oliveira Santos, F.; Pizzone, R. G.; Ryckewaert, G.; de Séréville, N.; Vanderbist, F. *Nucl. Phys. A* 2003, *716*, 211.

[23] Tang, Y. C.; LeMere, M.; Thompson, D. R. *Phys. Rep.* 1978, *47C*, 167.

[24] Adelberger, E. G.; García, A.; Robertson, R. G. H.; Snover, K. A.; Balantekin, A. B.; Heeger, K.; Ramsey-Musolf, M. J.; Bemmerer, D.; Junghans, A.; Bertulani, C. A.; Chen, J. W.; Costantini, H.; Prati, P.; Couder, M.; Uberseder, E.; Wiescher, M.; Cyburt, R.; Davids, B.; Freedman, S. J.; Gai, M.; Gazit, D.; Gialanella, L.; Imbriani, G.; Greife, U.; Hass, M.; Haxton, W. C.; Itahashi, T.; Kubodera, K.; Langanke, K.; Leitner, D.; Leitner, M.; Vetter, P.; Winslow, L.; Marcucci, L. E.; Motobayashi, T.; Mukhamedzhanov, A.; Tribble, R. E.; Nollett, K. M.; Nunes, F. M.; Park, T. S.; Parker, P. D.; Schiavilla, R.; Simpson, E. C.; Spitaleri, C.; Strieder, F.; Trautvetter, H. P.; Suemmerer, K.; Typel, S. *Rev. Mod. Phys.* 2011, *83*, 195.

[25] Baye, D. *Phys. Rev. C* 2004, *70*, 015801.

[26] Wang, C.; Cissé, O. I.; Baye, D. *Phys. Rev. C* 2009, *80*, 034611.

[27] Nagai, Y.; Igashira, M.; Takeda, K.; Mukai, N.; Motoyama, S.; Uesawa, F.; Kitazawa, H.; Fukuda, T. *Astrophys. J. Lett.* 1991, *372*, 683.

[28] Hesse, M.; Roland, J.; Baye, D. *Nucl. Phys. A* 2002, *709*, 184.

[29] Barker, F. C.; Kajino, T. *Aust. J. Phys.* 1991, *44*, 369.

[30] Baye, D. *Nucl. Phys. A* 2005, *758*, 114.

[31] Blatt, J. M.; Jackson, J. D. *Phys. Rev.* 1949, *76*, 18.

[32] Bethe, H. A. *Phys. Rev.* 1949, *76*, 38.

[33] Teichmann, T. *Phys. Rev.* 1951, *83*, 141.

[34] Hamilton, J.; Overbö, I.; Tromborg, B. *Nucl. Phys. B* 1973, *60*, 443.